RSC Advances

ROYAL SOCIETY OF CHEMISTRY

www.rsc.org/advances

Journal Name

RSCPublishing

ARTICLE

A Rapid Synthesis of TiO_2 Nanotubes in Ethylene Glycol System by Anodization as Pt-based Catalyst Support for Methanol Electrooxidation

Cite this: DOI: 10.1039/x0xx00000x

Received 00th January 2012,
Accepted 00th January 2012

DOI: 10.1039/x0xx00000x

www.rsc.org/

Xu-Lei Sui [a,b], Zhen-Bo Wang [a,*], Yun-Fei Xia [a], Min Yang [a], Lei Zhao [a], Da-Ming Gu [b*]

In this paper, we report a rapid method to synthesize the titania nanotubes as the support of Pt-based catalyst. The titania nanotubes can be obtained during 1200 s in ethylene glycol system by anodization method. Pt nanoparticles have been successfully deposited on the mixture of carbon and as-prepared TiO_2 nanotubes by a microwave-assisted polyol process. The electrochemical results show that the electrochemical active specific surface area and the activity of methanol electrooxidation for as-prepared catalyst are both much higher than those of commercial Pt/C. Whether it is through constant potential test or cycling potential test, the durability of as-prepared catalyst is higher than that of commercial Pt/C. Such remarkable performance are due to the strong corrosion resistance of titania, the metal support interaction and hydrogen spillover effect between Pt and titania, the better electronic conductivity, as well as the good dispersion of Pt nanoparticles. These studies indicate that titania nanotubes are promising catalyst support for methanol electrooxidation.

1. Introduction

Direct methanol fuel cell (DMFC) has attracted a large amount of attention as a promising power source for portable electronic devices and electric vehicles.[1, 2] The study and development of catalysts is an important part of this technology. Recently, the cathode catalysts have obtained significant progress due to the development of non-noble metal catalysts for the oxygen reduction reaction. Numerous efforts are devoted to the non-noble metal catalysts for cathode and the cost of cathode catalyst is greatly reduced.[3-5] However, so far, the noble metal Pt is still essential for the methanol electrooxidation. Therefore, how to improve the efficiency and lifetime of Pt-based catalyst for methanol electrooxidation is still an important issue.

The widely accepted method is to disperse Pt nanoparticles on large surface area supports.[6, 7] Currently, the carbon materials are frequently used for catalyst supports, including carbon black[8-10], carbon nanotube[11, 12] and graphene[13-15]. However, carbon corrosion leads to the decrease of catalytic performance during the long term operation of DMFC, especially in the case of the presence of active platinum.[16-18] Metal oxide supports are worthy desired supports due to not only the corrosion resistant in acidic and oxidative environments but the strong metal-support interaction with platinum, such as WO_3[19], SnO_2[20-22], TiO_2[23-25], CeO_2[26, 27] and so on. The metal-support interaction has been studied in detail by Lewera[28] and Zhang[29]. Further research done by Jaksic[30] shows the spillover effect on the enhancement of electrocatalytic performance for the interactive hypo-d-oxide supports. Titania has attracted increasing attention due to its low cost and environmental friendliness.[31] Nevertheless, the poor conductivity of titania restricts its application in fuel cell. In our previous work, it has been confirmed that titania nanotube can improve the electron conductivity of titania.[32] But the synthesis time of the titania nanotube is up to 3 h, and it is too long to the practical application. In this work, we rapidly fabricated the titania nanotubes during 1200 s in ethylene glycol system by the anodization method. Thus the usability of titania nanotubes for fuel cell is greatly improved. The Pt-based catalyst was prepared by a microwave-assisted polyol process and was characterized by physical and electrochemical measurements. These studies have shown that as-prepared catalyst exhbits better activity and durability for the methanol electrooxidation reaction than that of commercial Pt/C.

2. Experimental

2.1 Preparation of TiO_2 nanotube

Titania nanotubes (TNTs-EG) were fabricated by the anodization of Ti foils with the Pt sheet as the counter electrode. The Ti foils were ultrasonically degreased in acetone, isopropanol, methanol and deionized water, and then dried in air prior to anodization. The

anodization was carried out in a 500 mL beaker at room temperature at 120 V for 1200 s. The electrolyte was ethylene glycol solution of 0.1 mol·L^{-1} NH_4F, 5 *wt.* % H_2O and 1.5 mol·L^{-1} lactic acid. After anodization, the foils were washed for several times with deionized water and then dried. After scraped from the Ti foils, the samples were heated to 400 ^oC for 2 h in a Muffle furnace.

2.2 Preparation of Pt/C-TNTs-EG catalyst

20 *wt.* % Pt-based catalysts were synthesized by the typical microwave-assisted polyol process in ethylene glycol (EG) solution with H_2PtCl_6 as precursor salt. Briefly, the mixture of TNTs (20 mg) and Vulcan XC-72 carbon black (30 mg) were dispersed into the 25 mL mixed solution of ethylene glycol and isopropyl alcohol (V/V=4:1) under ultrasonic treatment for 1 h to form uniform suspension, and then adding an appropriate amount of H_2PtCl_6-EG solution with a subsequent stirring process for 3 h. The suspension was adjusted to pH 12.0 by using 1 mol·L^{-1} NaOH-EG solution. After argon gas was fed into the suspension for 15 min to expel oxygen, a subsequent microwave heating process was carried out for 55 s. The suspension was allowed to cool down to room temperature with continuous stirring, and then the pH value was adjusted to 2-3 for 12 h by HNO_3 aqueous solution. The product was washed repeatedly and filtered with ultrapure water (Millipore, 18.2 MΩ·cm). Lastly, the obtained catalyst was dried for 5 h at 80 ^oC in a vacuum oven and then stored in a vacuum vessel. All chemicals used were of analytical grade.

2.3 Characterizations of physical properties

A scanning electron microscope (SEM, Hitachi Ltd. S-4700) was used for morphological characterization of titania nanotubes. The X-ray diffraction (XRD) data was collected to characterize the crystal structure of the samples by a D/max-RB diffractometer (made in Japan) with a Cu Ka X-ray source, scanning between 10° and 90° at a rate of 4°·min^{-1}. Transmission electron microscopy (TEM) and high-resolution TEM (HRTEM) were carried out by a Japan JEOLJEM-2010EX transmission electron microscope with the applied voltage of 200 kV. X-ray photoelectron spectroscopy (XPS) analysis was carried out to detect the surface properties of samples using a Physical Electronics PHI model 5700 instrument, with Al X-ray source operating at 250 W.

2.4 Electrochemical measurements

Electrochemical experiments were carried out in a typical three electrodes cell at room temperature using a CHI 650E electrochemical analysis instrument. A platinum network and Hg/Hg_2SO_4 electrode (MSE) were used as the counter electrode and the reference electrode, respectively. A glassy carbon electrode with 4 mm diameter was used the working electrode. The electrolyte was the Ar-saturated 0.5 mol·L^{-1} H_2SO_4 solution as the supporting and the Ar-saturated 0.5 mol·L^{-1} H_2SO_4 containing 0.5 mol·L^{-1} CH_3OH solution for methanol electrooxidation.

The working electrode was fabricated as follows. 2.0 mg·mL^{-1} catalyst ink was formed by catalyst and ultrapure water. The 5μL catalyst ink was then pipetted onto the glassy carbon electrode. After drying, 5 μL dilute aqueous Nafion® solution was applied onto the surface of the catalyst layer to protect catalyst from detaching.

The cyclic voltammograms (CV) were recorded from -0.64 to 0.51 V *vs.* MSE at the rate of 50 mV·s^{-1}. Before measurements, the working electrode was firstly activated until a steady CV curve was obtained. The electrochemical active surface areas (ESA) of platinum were calculated with the formula $ESA=Q_H/(0.21*M_{Pt})$.[33] The amperometric *i–t* curves were obtained at a constant potential of 0.6 V *vs.* NHE for 3600 s in methanol acidic medium.

3. Results and discussion

3.1 Physical characterization of supports and catalyst

Fig. 1 shows the SEM image of as-prepared TNTs-EG by the anodization in the EG system. The structure of nanotube can be clearly seen, and the diameter and length of nanotubes can be easily measured. All the nanotubes have the similar pore structure with the average inner diameter of 90 nm and the average wall thickness of 10 nm. As evident in Fig. 1, the pores are uniform and closely packed. In addition, the length of nanotubes is not uniform among several hundred nanometers and several micrometers, and even some small fragments emerge. The different lengths may be due to the fracture of nanotubes when scraped off Ti foil. The broken structure can generate larger specific surface area, conducive to the deposition of Pt nanoparticles.

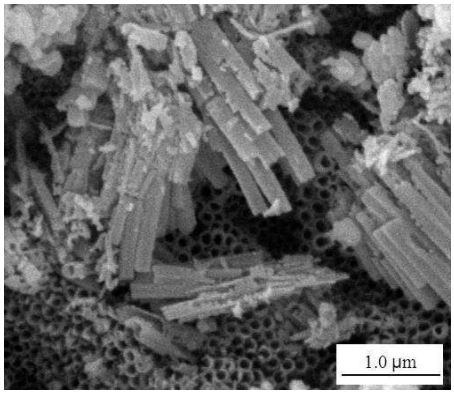

Fig.1 SEM image of as-prepared TNTs-EG by the anodization

The growth mechanism of TiO_2 nanotubes has been studied by many researchers.[34, 35] There are three processes, i.e., field-assisted oxidation at metal/oxide interface, field-assisted dissolution at oxide/electrolyte interface at tube bottom and chemical dissolution at tube mouth. The formation of nanotubes is a direct consequence of competition between the electrochemical etching rate and the chemical dissolution rate. The former rate is determined by field-assisted oxidation and dissolution. The latter rate is determined by chemical dissolution. In our work, the high applied potential enhances the ion migration in electrolyte and ion transport in anodic barrier layer, resulting in the rapid electrochemical etching rate. In the other hand, the adding of lactic acid promotes the chemical dissolution rate. Therefore, the thin layer of oxides on top of the nanotube arrays formed in the first few tens of seconds is rapidly

dissolved. At the same time, the balance of the electrochemical etching rate and the chemical dissolution rate can be attainable in a short time.

XRD was used to confirm the crystal phases of the TiO_2 nanotubes and the Pt-based catalysts. The results are shown in Fig. 2. After annealing at 400 °C, the as-prepared TiO_2 nanotubes are perfect anatase phase. The diffraction peaks are very sharp and corresponded with the standard spectrum. For the Pt/C-TNTs-EG catalyst, the diffraction peaks of anatase TiO_2 are remained and significant, which indicates that the synthesis process of catalyst has no influence on the crystallization of the TiO2 nanotubes. In addition, the representative diffraction peaks of Pt are unclear due to the suppression effect of TiO_2 strong peaks. However, the diffraction peak at $2\theta \approx 40°$ is significantly broadened, which is assigned to the overlapping of the Pt (111) diffraction peak. Similarly, the diffraction peak of amorphous carbon at $2\theta \approx 26°$ is unclear and only a small heave indicating the existence of carbon. The unstable base of Pt/C-TNTs-EG pattern is also the evidence for the presence of carbon.

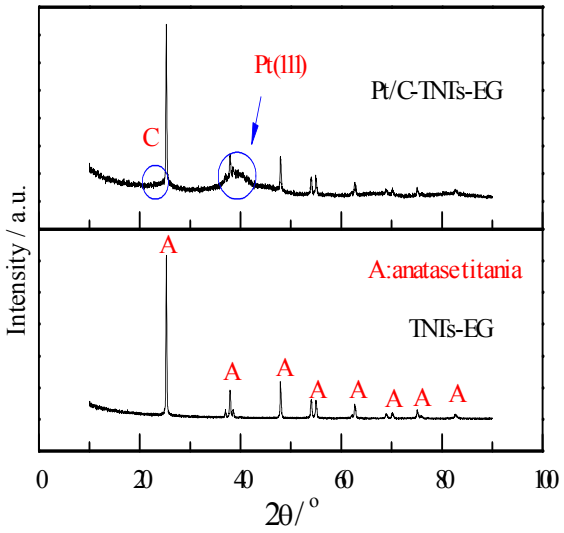

Fig. 2 XRD patterns of TNTs-EG and Pt/C-TNTs-EG

The morphology of the obtained samples is further determined by TEM as shown in Fig. 3a. The diameter of nanotube is about 110 nm and the length is inconsistent, which are consistent with the results of SEM. It is clearly seen that the distribution of Pt nanoparticles on TNTs-EG is very uniform which is beneficial to the improvement of catalyst. According to statistics based on the TEM, the associated size distribution of Pt nanoparticles is obtained and the mean size of Pt nanoparticles is about 2.4 nm as shown in Fig. 3b. The high-resolution TEM (HRTEM) image obtained from the red box region in Fig. 3a shows that the lattice fringes can be coherently extended across the whole area, indicating that the sample has good crystallization. As shown in Fig. 3c, the d-spacings of 0.35 nm and 0.23 nm correspond respectively to the (101) plane of the anatase TiO_2 and the (111) plane of face centered cubic Pt structure. Furthermore, the fast Fourier transform (FFT) pattern can confirm that the TiO_2 nanotube has a regular single crystal structure as shown in Fig. 3d.

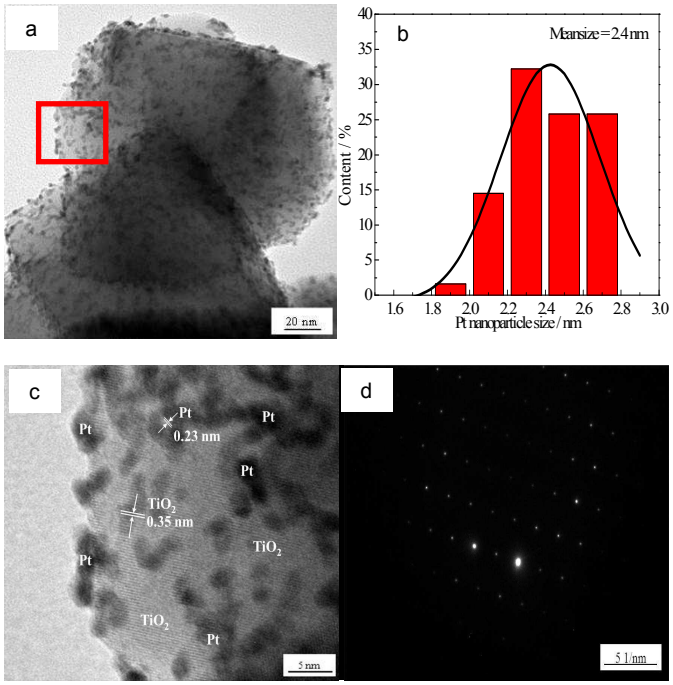

Fig. 3 TEM image of Pt/C-TNTs-EG (a); the size distributions of Pt nanoparticles (b); HRTEM image (c) and FFT pattern (d) of Pt/C-TNTs-EG

The chemical state information of Pt element in Pt/C-TNTs-EG is analyzed by X-ray photoelectron spectroscopy (XPS), and the commercial Pt/C is used as a comparison. As shown in Fig. 4, the Pt4f peak exhibits two associated peaks, representing the $Pt4f_{7/2}$ peak and the $Pt4f_{5/2}$ peak. The curve fitting of Pt4f peaks are carried out to gain the ratio of different valence and the deconvoluted results are shown in Tab. 1. The Pt (0) content of Pt/C-TNTs-EG and commercial Pt/C is similar, respectively 39.8 % and 41.0 %. However, the Pt (Ⅱ) and Pt (Ⅳ) contents of Pt/C-TNTs-EG and commercial Pt/C are distinctly different. The Pt (Ⅱ) content of Pt/C-TNTs-EG is much higher than that of commercial Pt/C while the Pt (Ⅳ) content of Pt/C-TNTs-EG is much lower. During the electrochemical activate stage, Pt (Ⅱ) is more easily converted to Pt (0) which could act as catalytic sites. Hence, Pt/C-TNTs-EG would exhibit higher catalytic performance than commercial Pt/C. In addition, the binding energy of Pt (0) for Pt/C-TNTs-EG shows a shift up of 0.18 eV in comparison with that of commercial Pt/C, indicating that there is a metal-support interaction (MSI) between Pt nanoparticles and titania. Specifically, there is a d-d-interelectronic bonding between Pt and TiO_2. The electron density on Pt decreases due to the altervalent changes ($Ti^{4+} \Leftrightarrow Ti^{3+}$) (equ.1 and equ.2)[30]. Therefore, the binding energy of Pt (0) shifts to higher energy, and it can be deduced that the Ti^{3+} concentration should increase in the presence of Pt. In fact, it has been shown that the concentration of Ti^{3+} is higher in the presence of Pt than on the pure support[36].

$$Ti(OH)_4 + Pt \rightarrow Ti(OH)_3^+ + Pt\text{-}OH + e^- \quad \text{equ.1}$$

$$Ti(OH)_3^+ + 2H_2O \rightarrow Ti(OH)_4 + H_3O^+ \quad \text{equ.2}$$

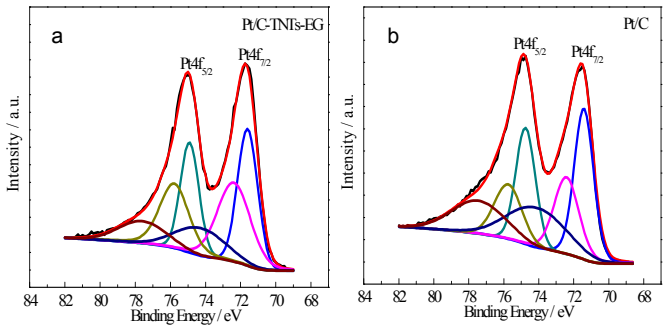

Fig. 4 the curve fittings of Pt4f peaks for Pt/C-TNTs-EG (a) and commercial Pt/C (b)

Tab. 1 the deconvoluted results of Pt4f peaks

Sample	Pt species	Binding energy	concentration
Pt/C-TNTs-EG	Pt (0)	71.60 eV	39.8 %
	Pt (Ⅱ)	72.38 eV	40.0 %
	Pt (Ⅳ)	74.29 eV	20.2 %
Pt/ C	Pt (0)	71.42 eV	41.0 %
	Pt (Ⅱ)	72.42 eV	27.7 %
	Pt (Ⅳ)	74.12 eV	31.3 %

3.2 Electrochemical measurement

Cyclic voltammograms (CV) of Pt/C-TNTs-EG is carried out in an Ar-saturated 0.5 mol·L^{-1} H_2SO_4 at a scanning rate of 50 mV·s^{-1} at 25 °C. The commercial Pt/C catalyst is used as a reference to evaluate the electrocatalytic performance of Pt/C-TNTs-EG. The results are shown in Fig. 5. It can be seen that both of curves have three typical regions described as the hydrogen region, the double layer region and the oxygen region. The electrochemical active specific surface area (ESA) is obtained by measurement of the hydrogen adsorption–desorption (HAD) integrals. The ESA of Pt/C-TNTs-EG is 91.8 $m^2 \cdot g^{-1}_{Pt}$, much higher than 56.3 $m^2 \cdot g^{-1}_{Pt}$ of commercial Pt/C. This demonstrates that the electrochemical activity of Pt/C-TNTs-EG catalyst is significantly higher than commercial Pt/C, which is ascribed to three major factors: (1) There is a metal-support interaction and hydrogen spillover effect between Pt nanoparticles and titania. (2) The adding of carbon greatly improves the electronic conductivity. (3) The dispersion of Pt nanoparticles on the titania nanotubes is uniform and the mean size of Pt nanoparticles is samll.

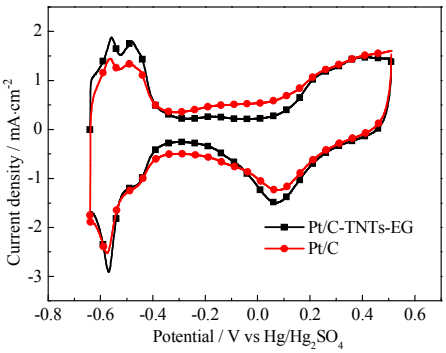

Fig. 5 Cyclic voltammogram of catalysts in 0.5 mol·L^{-1} H_2SO_4; the data of commercial Pt/C reproduced with permission[32]. Copyright2014, Elsevier.

We then evaluated the electrocatalytic performance of Pt/C-TNTs-EG for the methanol electrooxidation (MOR). The MOR measurements were performed in an Ar-saturated solution of 0.5 mol·L^{-1} H_2SO_4 containing 0.5 mol·L^{-1} CH_3OH at a scanning rate of 50 mV·s^{-1} at 25 °C. Fig. 6 shows the MOR curves for Pt/C-TNTs-EG and commercial Pt/C. We can see that the MOR curves display two distinguishable oxidation peaks. The forward peak current density is an important indicator with regard to methanol electrooxidation reaction. The forward peak current densities on the Pt/C-TNTs-EG and commercial Pt/C are 0.45 and 0.30 A·mg$^{-1}_{Pt}$, respectively, indicating that the activity of Pt/C-TNTs-EG is greatly high, which is about 1.5 times higher than that of commercial Pt/C. The results are consistent with their ESA above.

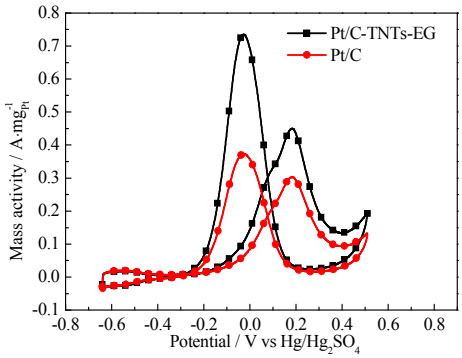

Fig. 6 Cyclic voltammogram of catalysts in methanol acidic medium; the data of commercial Pt/C reproduced with permission[32]. Copyright2014, Elsevier.

The CO-stripping experiment has been carried out as shown in Fig. 7. There is no significant difference in the onset potential of CO oxidation between Pt/C-TNTs-EG and commercial Pt/C. The reason may be as follows. The metal-support interaction induces the upshift of Pt binding energy for Pt/C-TNTs-EG, which simultaneously enhances the adsorption of OH and CO[30]. The enhanced adsorption of OH can promote the CO oxidation while the enhanced adsorption of CO can block the CO oxidation. The opposite effect possibly causes that the onset potential of CO oxidation for Pt/C-TNTs-EG does not shift. However, the metal-support interaction can weaken the adsorption of H, which is conducive to the efficient dehydrogenation on the Pt. In addition, the hydrogen spillover effect between Pt and TiO_2 can also promote the dehydrogenation reaction on the Pt, creating more clean active sites on the Pt.[37] Therefore, the electrochemical active specific surface area (ESA) and the activity of

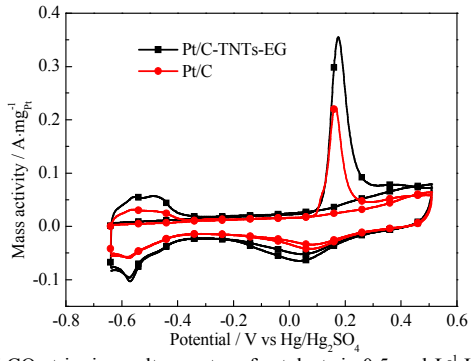

Fig. 7 CO-stripping voltammetry of catalysts in 0.5 mol·L^{-1} H_2SO_4

methanol oxidation for Pt/C-TNTs-EG are higher than those of commercial Pt/C.

We also evaluated the electrochemical durability of Pt/C-TNTs-EG by using constant potential test and cycling potential test in an Ar-saturated solution of 0.5 mol·L^{-1} H_2SO_4 containing 0.5 mol·L^{-1} CH_3OH at a scanning rate of 50 mV·s^{-1} at 25 °C. The amperometric *i–t* curves were obtained at a constant potential of 0.6 V *vs.* NHE for 3600 s as shown in Fig. 8. The final current densities after 3600 s are 22.2 and 7.6 mA·mg$^{-1}_{Pt}$, respectively, indicating that the activity of Pt/C-TNTs-EG is higher than commercial Pt/C. The durability of catalysts can be evaluated by calculating the ratio of the final current to the maximum current. The retention rates of mass current density are 19.3 % and 11.0 % for Pt/C-TNTs-EG and commercial Pt/C catalysts, respectively, revealing that the durability of Pt/C-TNTs-EG catalyst is higher than commercial Pt/C.

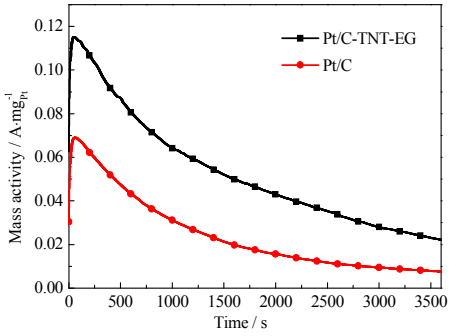

Fig. 8 the amperometric *i–t* curves of catalysts at a constant potential

The cycling durability behavior of Pt/C-TNTs-EG and commercial Pt/C catalysts toward methanol electrooxidation is evaluated, and the results of cycling aging test are shown in Fig. 9. The cycling potential is between -0.64 V to 0.51 V *vs.* MSE. From the normalized peak current density as shown in Fig. 9c, the retention rates of the peak current density are 70.1 % and 64.4 % for Pt/C-TNTs-EG and commercial Pt/C, respectively, after 600 cycles test. The result indicates that the durability of Pt/C-TNTs-EG is higher than that of commercial Pt/C. In addition, it is noteworthy that the peak current density of Pt/C-TNTs-EG is always much higher than that of commercial Pt/C during 600 cycles test as shown in Figure 9d. The initial activity of commercial Pt/C is equivalent to the activity of Pt/C-TNTs-EG after 600 cycles test. The result is exciting and hopeful for the future applications.

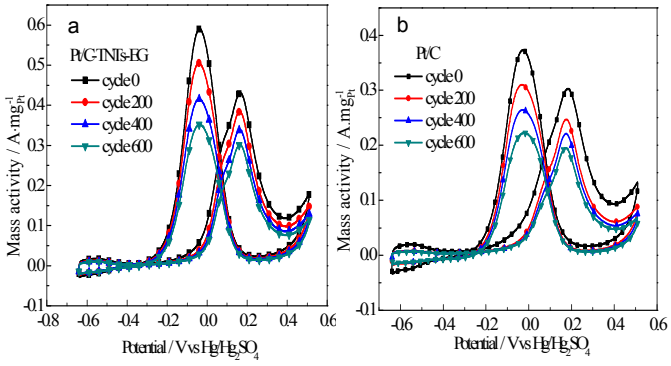

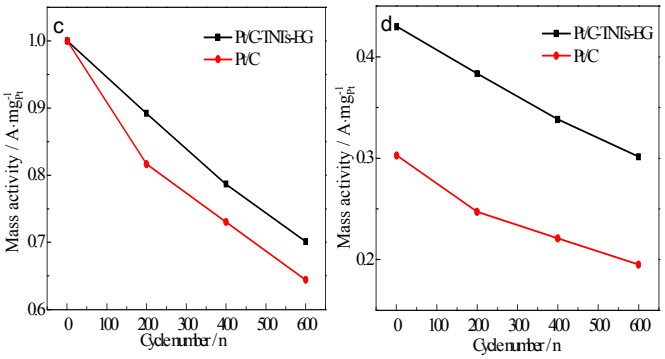

Fig. 9 cycling aging test of Pt/C-TNTs-EG (a) and commercial Pt/C (b); the relationship of peak current density and cycle number (c, d); the data of commercial Pt/C reproduced with permission[32]. Copyright2014, Elsevier.

4. Conclusions

In summary, titania nanotubes were rapidly fabricated by anodization method in ethylene glycol solution at 120 V for 1200 s. The Pt/C-TNTs-EG catalyst was prepared by a microwave-assisted polyol process and was characterized by physical and electrochemical measurements. These studies have shown that the Pt/C-TNTs-EG catalyst served as highly efficient catalysts for the methanol electrooxidation reaction with better activity and durability than commercial Pt/C. The enhanced performance could be attributed to the metal-support interaction and hydrogen spillover effect between Pt nanoparticles and titania, the high corrosion resistance of titania, the good electronic conductivity due to the adding of carbon, and the good dispersion of Pt nanoparticles on the titania nanotubes. The results reported herein suggest that titania nanotubes obtained from anodization is hopeful for the application in the future.

Acknowledgements

This research is financially supported by the National Natural Science Foundation of China (Grant No. 21273058), China postdoctoral science foundation (Grant No.2012M520731 and 2014T70350), Heilongjiang postdoctoral foundation (LBH-Z12089).

Notes and references

[a] School of Chemical Engineering and Technology, Harbin Institute of Technology, No.92 West-Da Zhi Street, Harbin, 150001 China. E-mail: wangzhb@hit.edu.cn; Tel.: +86-451-86417853; Fax: +86-451-86418616
[b] School of Science, Harbin Institute of Technology, No.92 West-Da Zhi Street, Harbin, 150001 China

1. A. Schroder, K. Wippermann, J. Mergel, W. Lehnert, D. Stolten, T. Sanders, T. Baumhofer, D. U. Sauer, I. Manke, N. Kardjilov, A. Hilger, J. Schloesser, J. Banhart and C. Hartnig, *Electrochem Commun*, 2009, **11**, 1606-1609.

2. A. Lam, D. P. Wilkinson and J. J. Zhang, *J Power Sources*, 2009, **194**, 991-996.
3. A. Morozan, B. Jousselme and S. Palacin, *Energy & Environmental Science*, 2011, **4**, 1238-1254.
4. H. R. Byon, J. Suntivich and Y. Shao-Horn, *Chem Mater*, 2011, **23**, 3421-3428.
5. R. Othman, A. L. Dicks and Z. H. Zhu, *Int J Hydrogen Energ*, 2012, **37**, 357-372.
6. V. Selvaraj and M. Alagar, *Electrochem Commun*, 2007, **9**, 1145-1153.
7. C. P. Liu, X. Z. Xue, T. H. Lu and W. Xing, *J Power Sources*, 2006, **161**, 68-73.
8. C. L. Hui, X. G. Li and I. M. Hsing, *Electrochim Acta*, 2005, **51**, 711-719.
9. W. Li, X. S. Zhao, T. Cochell and A. Manthiram, *Appl Catal B-environ*, 2013, **129**, 426-436.
10. C.-Z. Li, Z.-B. Wang, J. Liu, C.-T. Liu, D.-M. Gu and J.-C. Han, *Rsc Advances*, 2014, **4**, 63922-63932.
11. X. Wang, W. Z. Li, Z. W. Chen, M. Waje and Y. S. Yan, *J Power Sources*, 2006, **158**, 154-159.
12. L. Zhao, Z.-B. Wang, X.-L. Sui and G.-P. Yin, *J Power Sources*, 2014, **245**, 637-643.
13. M. Chen, Y. Meng, J. Zhou and G. W. Diao, *J Power Sources*, 2014, **265**, 110-117.
14. Y. J. Hu, P. Wu, Y. J. Yin, H. Zhang and C. X. Cai, *Appl Catal B-environ*, 2012, **111**, 208-217.
15. D. Bin, F. Ren, H. Wang, K. Zhang, B. Yang, C. Zhai, M. Zhu, P. Yang and Y. Du, *Rsc Advances*, 2014, **4**, 39612-39618.
16. K. H. Kangasniemi, D. A. Condit and T. D. Jarvi, *J Electrochem Soc*, 2004, **151**, E125-E132.
17. E. Guilminot, A. Corcella, M. Chatenet, F. Maillard, F. Charlot, G. Berthome, C. Iojoiu, J. Y. Sanchez, E. Rossinot and E. Claude, *J Electrochem Soc*, 2007, **154**, B1106-B1114.
18. J. J. Wang, G. P. Yin, Y. Y. Shao, S. Zhang, Z. B. Wang and Y. Z. Gao, *J Power Sources*, 2007, **171**, 331-339.
19. A. U. Rehman, S. S. Hossain, S. U. Rahman, S. Ahmed and M. M. Hossain, *Appl Catal A-Gen*, 2014, **482**, 309-317.
20. J. W. Magee, W. P. Zhou and M. G. White, *Appl Catal B-environ*, 2014, **152**, 397-402.
21. E. Higuchi, T. Takase, M. Chiku and H. Inoue, *J Power Sources*, 2014, **263**, 280-287.
22. A. Sandoval-Gonzalez, E. Borja-Arco, J. Escalante, O. Jimenez-Sandoval and S. A. Gamboa, *Int J Hydrogen Energ*, 2012, **37**, 1752-1759.
23. Z. Z. Jiang, Z. B. Wang, Y. Y. Chu, D. M. Gu and G. P. Yin, *Energy & Environmental Science*, 2011, **4**, 728-735.
24. B. Y. Xia, S. Ding, H. B. Wu, X. Wang and X. W. Lou, *Rsc Advances*, 2012, **2**, 792-796.
25. W. L. Qu, Z. B. Wang, X. L. Sui, D. M. Gu and G. P. Yin, *Int J Hydrogen Energ*, 2012, **37**, 15096-15104.
26. Y.-Y. Chu, Z.-B. Wang, Z.-Z. Jiang, D.-M. Gu and G.-P. Yin, *Adv Mater*, 2011, **23**, 3100-3104.
27. C. L. Menendez, Y. Zhou, C. M. Marin, N. J. Lawrence, E. B. Coughlin, C. L. Cheung and C. R. Cabrera, *Rsc Advances*, 2014, **4**, 33489-33496.
28. A. Lewera, L. Timperman, A. Roguska and N. Alonso-Vante, *J Phys Chem C*, 2011, **115**, 20153-20159.
29. D.-Y. Zhang, Z.-F. Ma, G. Wang, K. Konstantinov, X. Yuan and H.-K. Liu, *Electrochem Solid State Lett Electrochem. Solid State Lett.*, 2006, **9**, A423-A426.
30. J. A. Jaksic, N. V. Krstajic, L. M. Vracar, S. G. Neophytides, D. Labou, P. Falaras and M. M. Jaksic, *Electrochim Acta*, 2007, **53**, 349-361.
31. Z. M. Liu, J. L. Zhang, B. X. Han, J. M. Du, T. C. Mu, Y. Wang and Z. Y. Sun, *Micropor Mesopor Mater*, 2005, **81**, 169-174.
32. X. L. Sui, Z. B. Wang, M. Yang, L. Huo, D. M. Gu and G. P. Yin, *J Power Sources*, 2014, **255**, 43-51.
33. Y. C. Xing, *J Phys Chem B*, 2004, **108**, 19255-19259.
34. L. Sun, S. Zhang, X. W. Sun and X. He, *J Electroanal Chem*, 2009, **637**, 6-12.
35. Z. B. Xie and D. J. Blackwood, *Electrochim Acta*, 2010, **56**, 905-912.
36. F. Pesty, H. P. Steinruck and T. E. Madey, *Surf Sci*, 1995, **339**, 83-95.
37. S. J. Yoo, K.-S. Lee, Y.-H. Cho, S.-K. Kim, T.-H. Lim and Y.-E. Sung, *Electrocatalysis*, 2011, **2**, 297-306.

A Rapid Synthesis of TiO_2 Nanotubes in Ethylene Glycol System by Anodization as Pt-based Catalyst Support for Methanol Electrooxidation

Xu-Lei Sui, Zhen-Bo Wang, Yun-Fei Xia, Min Yang, Lei Zhao, Da-Ming Gu

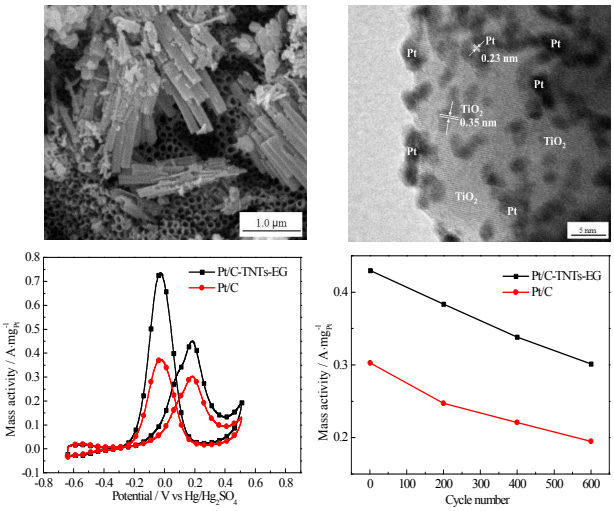

titania nanotubes were rapidly fabricated by anodization method in ethylene glycol solution and used as Pt-based catalyst support. The dispersion of Pt nanoparticles on titania nanotubes is very uniform. The as-prepared catalyst exhibits much higher electrochemical activity and durability than commercial Pt/C.